Cement & Concrete Composites 55 (2015) 122–128

Contents lists available at ScienceDirect

Cement & Concrete Composites

journal homepage: www.elsevier.com/locate/cemconcomp

Investigation of crushed brick-matrix interface in lime-based ancient mortar by microscopy and nanoindentation

V. Nežerka [a,*], J. Němeček [a], Z. Slížková [b], P. Tesárek [a]

[a] Faculty of Civil Engineering, Czech Technical University in Prague, Thákurova 7, 166 29 Praha 6, Czech Republic
[b] Institute of Theoretical and Applied Mechanics AS CR, Prosecká 76, 190 00 Praha 9, Czech Republic

ARTICLE INFO

Article history:
Received 26 September 2013
Received in revised form 16 July 2014
Accepted 28 July 2014
Available online 30 September 2014

Keywords:
Nanoindentation
Historic mortars
Cocciopesto
Reaction rim
ITZ

ABSTRACT

Lime-based mortars containing crushed clay bricks were widely used in history and proved to be more durable than other binding materials, especially when used in seismic areas. So far, their enhanced strength and durability have been attributed to the formation of hydration products on the interface between the lime-based matrix and brick fragments. These conclusions have been exclusively reached on the basis of macroscopic mechanical tests and local chemical analyzes of mortar constituents, while the local mechanical analyzes were lacking. The purpose of this paper is to verify the previous measurements and to quantify the elastic properties of the interfacial transition zone (ITZ) between crushed brick fragments and the surrounding matrix by means of nanoindentation, complemented by microscopy investigations. To that goal, an ancient mortar sample from a late Byzantine church was investigated. The elemental analysis revealed an increased amount of silica and alumina in the vicinity of brick fragments in relation to the matrix composition. In addition, an increased stiffness of ITZ compared to the lime matrix in the distance up to 20–30 μm from the grains was encountered by nanoindentation. Therefore, it was confirmed that the interface is stronger than the surrounding matrix, unlike the situation of inert sand aggregates, where ITZ is weakened by shrinkage-induced cracking. The average Young's modulus in ITZ assessed by nanoindentation (18.4 GPa) was comparable with low-density C-S-H phases that appear in cementitious composites. The information contained in this paper contribute to a better understanding of traditional mortars and provide the input data for their further micromechanical modeling.

1. Introduction

The use of lime as a binder in mortars is connected with many obstacles such as slow setting, high shrinkage and low mechanical strength [1]. These inconveniences can be overcome by the introduction of silica (SiO_2) and alumina (Al_2O_3), forming calcium silicates and aluminates [2], into the mortar in form of additives, called pozzolans. Pozzolanic mortars are able to harden in high relative humidity (therefore they are categorized as *hydraulic*) and also when the access of CO_2 is limited [3]. The presence of pozzolanic minerals in lime binder also improves the cohesion between the binder and aggregates and consequently also the mortar strength [1,3]. In general, pozzolanic materials containing large proportions of amorphous silico-aluminates and particles of small diameter exhibit high reactivity [4].

Powdered ceramic material was used as a pozzolanic material since the early Hellenistic period. The Romans added crushed bricks into the mortar when there was no volcanic material available in the region and called such material *cocciopesto* [5]. Crushed bricks were frequently added into the lime-based mortars during the Byzantine period [6], and these were preferred in water-bearing structures and to protect the walls from moisture, typically in baths [7], canals and aqueducts [8,9]. It has been reported in a few papers [10–12] that a thin layer of hydration products forms around the crushed ceramic particles if the clay is fired at appropriate temperature between 600 and 900 °C so that the clay minerals can gain the pozzolanic activity [13]. Based on the mineralogical composition, it was only assumed that the layer of hydration products strengthens the composite and improves the bond with the surrounding matrix. However, due to the limited thickness of the interfacial transition zone (ITZ), conventional testing methods cannot be used for investigation of its mechanical properties and to prove this hypothesis.

The purpose of this work is to investigate the boundary of crushed brick fragments and ITZ between the surrounding lime-

* Corresponding author.
E-mail addresses: vaclav.nezerka@fsv.cvut.cz (V. Nežerka), jiri.nemecek@fsv.cvut.cz (J. Němeček), slizkova@itam.cas.cz (Z. Slížková), tesarek@fsv.cvut.cz (P. Tesárek).

http://dx.doi.org/10.1016/j.cemconcomp.2014.07.023
0958-9465/

based matrix, and to asses the elastic properties of ITZ by nanoindentation. This method, originally developed for testing of homogenous materials, is now widely used also for quantification of mechanical properties of various composites including cement or lime based mortars.

Among others, nanoindentation had been recently exploited by Hughes and Trtik [14] for assessment of micromechanical properties of cement paste, Constantinides and Ulm [15] utilized nanoindentation to determine the elastic modulus of high and low density C-S-H gel, and Němeček et al. [16] exploited the grid nanoindentation for identification of individual phases in cement pastes and aluminum alloys, and Tesárek et al. [17,18] used similar technique for identification of phases in gypsum. Statistical analysis is mostly employed for the analysis of multi-phase structural materials [19,20]. An indirect approach was used by Neubauer et al. [21], who determined the elastic properties of interfacial transition zone (ITZ) around aggregates in concrete by fitting the microstructural model to experimental data.

2. Materials

The investigated sample was extracted from the apse of a late Byzantine church built approximately in the 9th century AD in the district Üsküdar, located in Istanbul, Turkey. The sample of the bedjoint mortar contained pieces of crushed bricks, which represented the main type of the aggregate, Fig. 1a. Beside the brick fragments, the mortar contained also particles of porous slag, polycrystalline quartz, and grains of laminated and micritic carbonate (calcite). The binder to aggregate ratio in the investigated mortar sections was approximately equal to 2 : 3 by volume as provided by the image analysis performed on area approximately 20 × 20 mm.

The chemical composition of the mortar sample was investigated by means of the Scanning Electron Microscopy/Energy Dispersive X-ray Spectroscopy (SEM-EDX) and the results are summarized in Table 1. The analysis was focused on the composition of the lime-based matrix, the unreacted core of crushed brick fragments (dark center of the brick fragment in Fig. 1a), reaction rim formed at their boundary (light colored in Fig. 1a) and ITZ around the fragments; the location of individual phases is indicated in Fig. 1b.

The results summarized in Table 1 were obtained as an average of several area measurements on areas of about 150 × 150 μm at distinct locations within individual phases. Approximately 20 analyzes were performed for each phase (brick, reaction rim, ITZ and matrix) on the surface of 3 polished thin mortar sections. The matrix phase was chemically most homogeneous, while the brick fragments exhibited the highest variations in terms of the elemental composition.

Table 1
SEM-EDX analysis of mortar components.

Component	Amount [% by weight] (±2.0%)			
	Matrix	ITZ	Brick reaction rim (light)	Unreacted brick (dark)
CaO	57.1	57.3	36.3	15.6
SiO_2	31.0	34.5	39.9	56.8
Al_2O_3	8.72	8.81	10.2	14.8
MgO	1.50	1.26	3.42	1.31
K_2O	–	–	1.74	2.87
Na_2O	–	–	0.37	3.64
FeO	–	–	7.29	4.99
TiO_2	–	–	1.53	0.53
SO_3	1.17	–	0.66	–

3. Morphological and chemical analyzes

Thin sections of the mortar samples were investigated by petrographic microscopy (Zeiss NU2 microscope) and scanning electron microscopy (SEM). Petrographic microscopy (PM) in linear polarized light mode, under crossed polars (XPL) and reflected polarized light (RPL) was used to analyze the general texture of the mortar and the reaction patterns. For higher resolution imaging and micro chemical analysis SEM was utilized. The SEM study in backscatter mode and micro chemical analysis with an energy dispersive X-ray detector (EDX) attached to the SEM were performed using MIRA II LMU device produced by Tescan Corporation with EDX by Bruker Corporation. The polished sections were coated with a thin layer of carbon in order to increase the conductivity necessary for a high resolution of the images.

The crushed brick aggregate was composed of fragments having their size in the range 0.5–12 mm with sub-angular surface texture and various red color shades. Some brick grains showed reaction rims indicated by the changes of red color in PM (Fig. 1a) and reduced porosity revealed by SEM (Fig. 1b). Based on the PM and SEM image analysis, the thickness of the rims was established as 100–200 μm. The chemical composition of the distinct phases was investigated separately and the results are summarized in Table 1.

The matrix phase was intensively cracked and it is represented mainly by a gray-green color in the PM images, see Fig. 2a. Its composition, determined by SEM-EDX analysis, is relatively homogeneous and can be classified as eminently hydraulic lime, see Table 1. Fig. 2a also shows the calcium carbonate particles, repre-

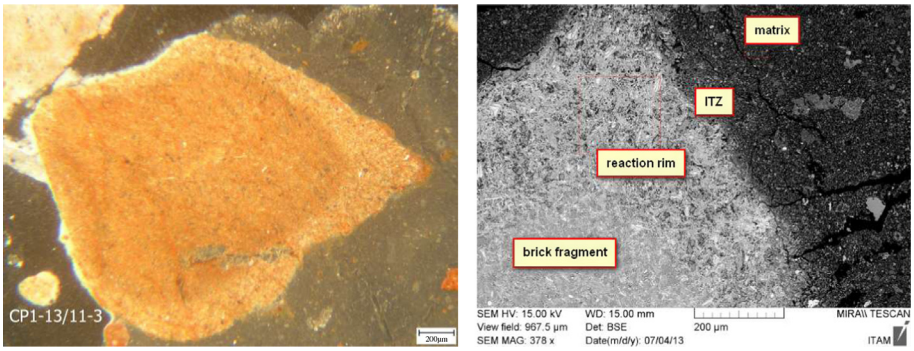

(a) brick grain surface texture with a reaction rim of various thickness (RPL), magnified 500×, scale bar = 200 μm

(b) SEM-BSE micrograph of brick fragment boundary, magnified 378×

Fig. 1. Presence of reaction rims at boundary of crushed brick particle.

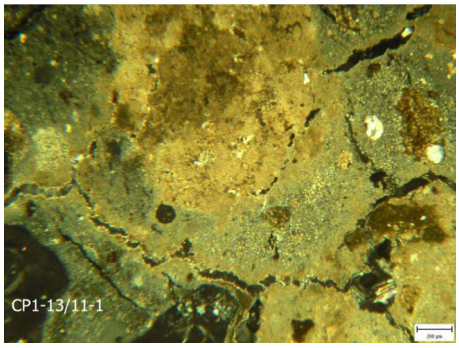

(a) Detail of cracked mortar binder (XPL), magnified 500×, scale bar = 200μm

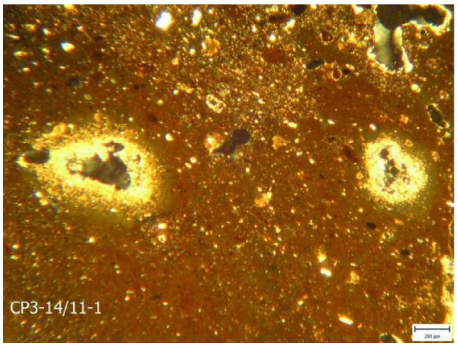

(b) Brick structure with oval pores partially filled with yellow clay and new minerals growing in the cavities (RPL), magnified 500×, scale bar = 200 μm

Fig. 2. Texture of crushed bricks and surrounding matrix.

sented by the brown area at the top of the figure. These particles were not present in a high concentration and consisted mainly of CaO (93%), which was determined by SEM-EDX.

Beside crushed bricks, the mortar contained also some other particles as gray porous isotropic slags, volcanic rocks with porphyric structure (Fig. 3a), grains of polycrystalline quartz (Fig. 3b), carbonates with polysynthetic lamination (Fig. 3c) and grains of micritic carbonate. However, the reaction rims were observed only at the boundary of crushed brick fragments.

The main attention of the present study was paid to the interface (ITZ) between the lime-based matrix and crushed brick particles which is assumed, as expected from previous studies, to have a significant influence on the mortar mechanical performance [21,22]. Probably multiple reasons positively influenced the development of the reinforced ITZ and reaction rims at the boundary of crushed brick fragments. Namely, these are wet environment, which is crucial for the activation of pozzolans and formation of hydration products [3,8,9], the suitable mineralogical composition of matrix and crushed particles rich in aluminosilicates [4] (see Table 1), and also the mortar age [23].

Elemental mapping by SEM-EDX was utilized to study the distribution of basic elements in composite components and reaction compounds. With respect to the inhomogeneous chemical composition of the individual phases, mainly the distribution of elements present in the highest concentrations (Ca, Al and Si) is discussed. As the content of Si an Al decreases from bricks to the matrix, an opposite trend was found in the case of Ca distribution. Beside these elements, the mortar matrix was relatively rich in magnesium and sulphur, and unlike in the case of brick fragments and reaction rims, the presence of alkali elements (Na and K) was not detected. Fe element was not present in the matrix phase and its distribution within brick fragments was highly nonhomogeneous.

The change in concentration of CaO and aluminosilicates (SiO_2 and Al_2O_3) within a section through the matrix and brick fragment is indicated in Fig. 1b. Figs. 4 and 5 show the microstructure and elemental composition of the brick-binder interface. The elemental maps revealed an aluminum and silicon enrichment in the interface area as a result of the hydraulic reaction between the both components, Figs. 4b and 5b. The Ca element is present in relatively high concentrations within the reaction rim (Fig. 5c), due to filling of voids by CaO. These findings support the hypothesis of calcium silicates and aluminates formation within the ITZ and reduction of pore radii at the boundary of brick fragments, which is in accordance with other studies [12,24,25].

4. Nanoindentation

Micromechanical properties of ITZ were studied by means of nanoindentation. Nanohardness tester (CSM Instruments, Switzerland) equipped with Berkovich (pyramidal) diamond tip was utilized for all measurements. The instrument is capable of performing indentations located in pre-defined positions via coupled optic system with ≈0.5 μm precision and with maximum load capacity 500 mN.

The sample was sectioned and mechanically polished prior to the measurement. A series of abrasive SiC papers with grits down to #4000 were used. Suspension containing 0.25 μm diamond particles was applied in the final polishing stage and all the dust and

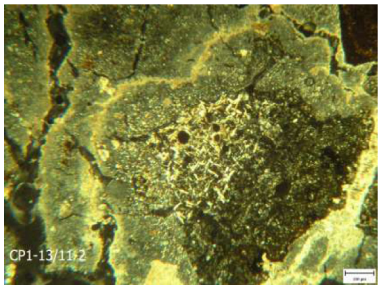

(a) volcanic rock (center) and black isotropic slag (right), scale bar = 300 μm

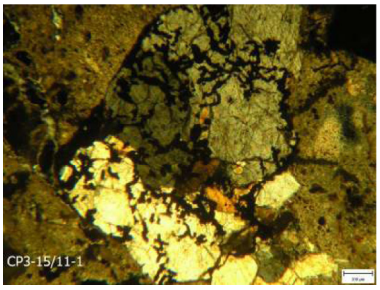

(b) polycrystalline quartz grain in mortar binder, scale bar = 300 μm

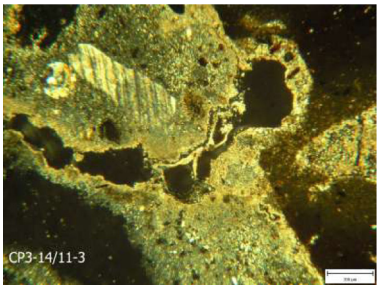

(c) grain of carbonate with polysynthetic lamination (upper part), scale bar = 300 μm

Fig. 3. XPL analysis of non-brick aggregates.

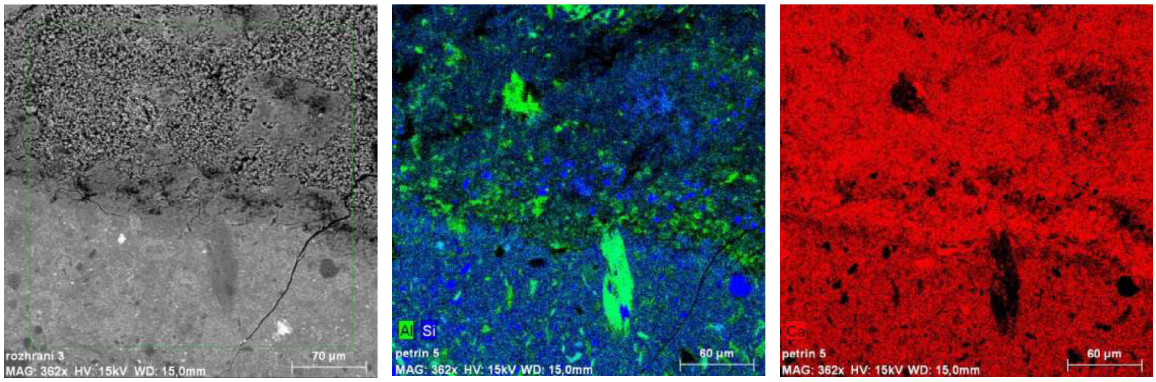

(a) Interface between brick (bottom) and matrix (top), scale bar = 70 µm

(b) Al and Si (green and blue) distribution around ITZ, scale bar = 60 µm

(c) Ca (red) distribution around ITZ, scale bar = 60 µm

Fig. 4. BSE image and SEM-EDX elemental maps, magnified 362×.

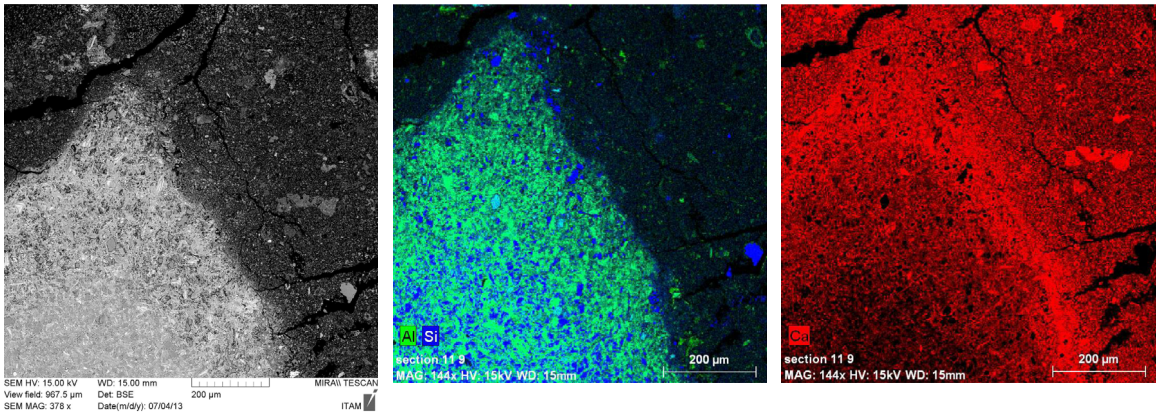

(a) Interface between brick (bottom) and matrix (top), scale bar = 200 µm

(b) Al and Si (green and blue) distribution around ITZ, scale bar = 200 µm

(c) Ca (red) distribution around ITZ, scale bar = 200 µm

Fig. 5. BSE image and SEM-EDX elemental maps, magnified 144×.

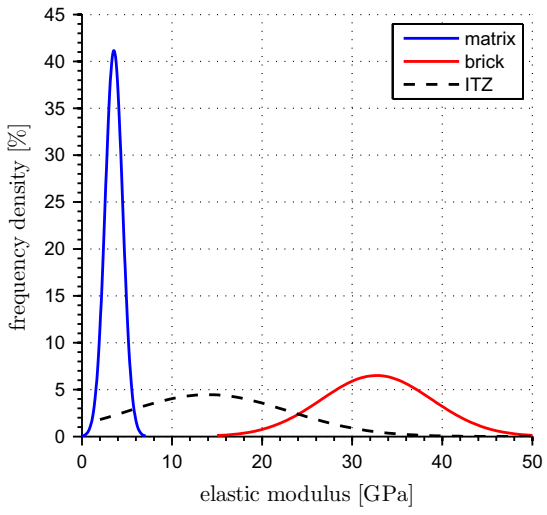

Fig. 6. Gauss distributions of Young's modulus in matrix and brick fragments.

free particles were removed from the surface of the samples by alcohol and simultaneous action of an ultrasonic bath.

A suitable ITZ location with minimum roughness was selected optically before the measurement. Several rectangular grids, each containing three parallel rows of indents, were placed at the brick-matrix interface. The size of individual indents and their spacing within the grid were chosen to minimize their mutual influence but to capture the gradient of mechanical behavior. The penetration depth of individual indents had to be chosen relatively large in order to avoid the influence of roughness, which is relatively high compared to e.g. more compact cementitious composites. The total area covered by a single indentation grid was prescribed to be 70×21 µm (with the larger dimension directed perpendicular to the interface). The spacing of indents was set to 7 µm in both directions. The arrangement of indents is illustrated in Fig. 7.

Load controlled quasi-static indentation test was employed for all imprints within the grid. Loading function containing three segments (constant loading at 24 mN/min, holding period 10 s, and unloading at 24 mN/min) was used for each location and maximum load was set to 2 mN. The holding period was included to

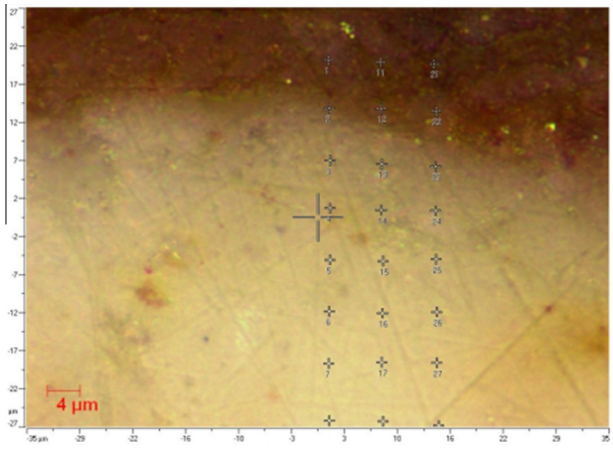

Fig. 7. Detail of ITZ with prescribed indents locations as seen in optical microscope (brick at top), scale bar = 4 μm.

reduce creep effects on the elastic unloading [26]. The penetration depth varied depending on the stiffness of the indented phase.

Relatively large stiffness of the brick caused small penetration depths of indents (≈270 nm) in this part of the indentation grid. The penetration depth increased in matrix as the stiffness was decreasing from the brick interface. An average indentation depth outside the brick phase reached ≈900 nm. The penetration depth is associated with the affected indentation volume from which mechanical response is obtained. It must be understood that the mechanical stiffness obtained from indentation tests includes also all inhomogeneities in this volume (including porosity). Thus, the elastic constants received from the tests must be treated as effective values of the indentation volume, and the effective depth influenced by the indenter tip can be roughly estimated as three times the penetration depth which yields ≈2.7 μm.

According to Arizzi and Cultorne [1] the majority of pores present in hydraulic lime mortars is having their diameter in range between 0.01 and 0.1 μm. This has been supported by the findings by Lawrence et al. [27] who claim that the pores having the diameter approximately 0.1 μm are formed in all lime-based mortars, since these are attributed to the transformation of portlandite ($Ca(OH)_2$) to calcite ($CaCO_3$). The hydraulic mortars have generally their pores shifted towards smaller radii around 0.03 μm [2,28,29]. This is in agreement with our measurement based on mercury intrusion porosimetry (MIP), which indicated that all the pores within the sample were having the diameter lower than 0.9 μm and the highest frequency was found for pores of diameter equal to 0.5 μm. From this point of view the effective nanoindentation depth about ≈2.7 μm ensured sufficient volume of the material to include all pores in the micrometer range that are detectable by MIP.

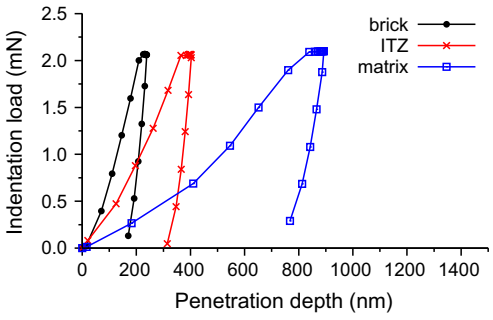

Fig. 8. Typical examples of loading diagrams obtained at different locations within matrix by nanoindentation.

The typical example of indentation loading curves corresponding to different components, i.e. the matrix, brick fragment and ITZ, are depicted in Fig. 8. It is clear from Fig. 8 that the stiffest response (characterized with the steepest unloading slope of the curve) is represented by the brick phase, ITZ is characterized with an intermediate stiffness, and the matrix is the most compliant part of the composite.

Each indent was evaluated by using the Oliver and Pharr methodology [30] which utilizes the unloading part of the indentation curve for the assessment of the material elastic modulus. From an experiment, the indentation (reduced) modulus is received as:

$$E_r = \frac{1}{2\beta}\frac{\sqrt{\pi}}{\sqrt{A}}\frac{dP}{dh} \tag{1}$$

in which P is the indentation force, h is the penetration depth, $\frac{dP}{dh}$ is the contact stiffness, β is a geometrical factor introduced to correct non-symmetrical shape of an indenter (1.0 for a spherical tip, 1.034 for Berkovich indenter) and A is a projected contact area of the indenter. The reduced modulus is then converted to Young's modulus of the tested material from the series combination of plane strain moduli of the two bodies in contact (i.e. the sample and the indenter) as:

$$\frac{1}{E_r} = \frac{(1-\nu^2)}{E} + \frac{(1-\nu_i^2)}{E_i} \tag{2}$$

where ν is Poisson's ratio of the measured material, and E_i and ν_i are elastic modulus and Poisson's ratio of the indenter, respectively.

Constant Poisson's ratio representing the indented phases, and equal to 0.2, was considered within the evaluation, also assuming isotropic character of the indented phase. Quite consistent results from all tested locations were obtained and no major differences occurred among the grids. Elastic moduli were averaged from respective positions in a grid and the resulting evolution of elastic stiffness in ITZ can be seen in Fig. 9a. It is characterized by a steep decrease from the brick modulus (average ≈32.7 GPa) to the average matrix modulus (3.6 GPa). The gradient of the stiffness occurs in a narrow 20–30 μm band at the brick phase. The width of this stiffness gradient agrees well with SEM images providing the information about the thickness of reaction rims.

Independent nanoindentation measurements were also performed on pure brick and matrix phases at regions located in sufficient distance from the ITZ using the same loading conditions. Elastic parameters of the distinct phases were characterized with high variations which is typical of these highly inhomogeneous

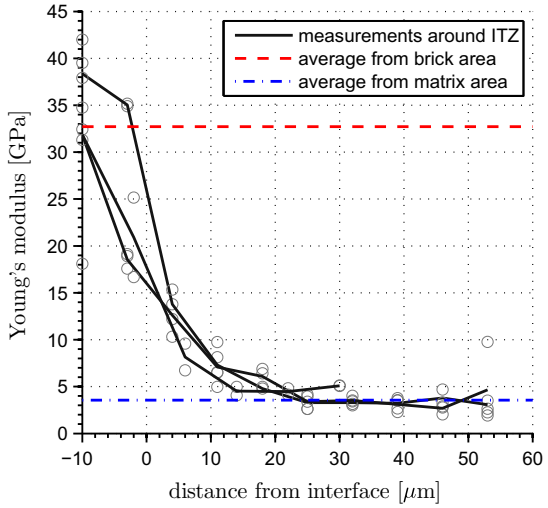

Fig. 9. Development of elastic stiffness around brick-matrix interface.

Table 2
Young's modulus of matrix and brick fragments.

	Matrix	Brick	ITZ
Satisfactory indents	30	46	21
Mean Young's modulus (GPa)	3.6	32.7	18.4
C.O.V. (%)	27.3	18.7	63.8

materials. The parameters are summarized in Table 2 together with the results of the measurements in the expected location of ITZ, in the distance 0–30 μm from the interface of brick fragments. The Gaussian distributions of Young's moduli evaluated from individual indents within matrix and brick fragment are depicted in Fig. 6. The development of Young's modulus in dependence on the distance from the brick interface can be seen in Fig. 9a and it is complemented by Fig. 10 showing the development of element distribution in individual phases.

5. Results and discussion

The investigated sample of the ancient mortar consisted of brick fragments, slag, some other rocks grains and the predominantly hydraulic lime binder. The amorphous components of the crushed brick aggregates are generally mainly represented by aluminosilicates, which react with lime because the lime makes the interfacial surface alkaline. Resulting products of the chemical reaction, taking place at the interface between ceramic particles and the lime-based matrix, are calcium silicate hydrate (CSH) and/or calcium-aluminate-hydrate (CAH), giving the mortars a hydraulic character [25]. This was confirmed by SEM and PM analyzes, where the reaction rims of the thickness 100–200 μm at the boundary of brick fragments and the reinforcement of ITZ in the thickness of 20–30 μm were observed.

Similar study was performed by Moropoulou et al. [10] in depth over a range of 120 μm, going from a matrix to a brick phase and considering the interface in thickness ranging from 30 to 50 μm. It revealed the following significant features: Ca element decreases, while Si and Al compounds increase from mortar matrix to brick. This was confirmed by our study, in which the CaO filling the pores of crushed brick fragments in the thickness up to 200 μm was observed, and the presence of aluminosilicates at the expense of the calcium was detected within ITZ in the thickness approximately 20–30 μm. That confirms the idea of Moropoulou et al. [12] that the lime penetrates into the ceramic and the consequent reaction transforms the microstructure of the ceramic by reduction

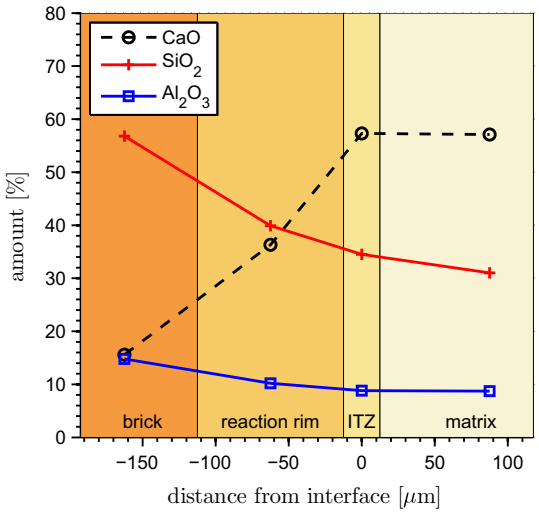

Fig. 10. Amount of calcite and aluminosilicates in individual phases.

of pore radii. However, in the case of large sized brick pebbles, the reaction cannot penetrate very far into the pebble and the reaction can only result in a better adhesion between the binder and the aggregate [31].

The reduction of porosity and the slightly higher amount of aluminosilicates within ITZ have an impact on its mechanical properties and influence the mechanical properties of mortars, as provided by micromechanical studies, e.g. [22,32]. Therefore, the stiffness of ITZ was investigated by means of nanoindentation, providing the information about the stiffness of the matrix, brick fragments and the interface between these two distinct phases. Relatively high scatter of the results indicates that both phases are highly inhomogeneous, but distinct enough to capture their boundary. There was clearly observed ITZ, represented by the gradient of measured stiffness, located in a narrow, 20–30 μm, band at the boundary of brick fragments. It is in a perfect agreement with the results provided by SEM-EDX analysis.

It was reported that mortar samples containing crushed bricks exhibit self-healing effects thanks to the presence of the amorphous hydraulic calcium-silicate-hydrate (CSH) formations [10]. This idea is supported, beside SEM-EDX analysis, by the results of our nanoindentation measurements, yielding the stiffness of ITZ (18.4 GPa) similar to the stiffness of low-density CSH found in cement pastes [19,26].

Moropoulou et al. [33] suggested that the presence of CSH gels could contribute to the increased resistance of cocciopesto mortars to earthquakes, since they require a higher energy absorption without initiations of fractures. According to our measurement the formation of hydration products reinforces ITZ and contributes to a better adhesion between the brick fragments and the surrounding matrix, unlike in case of inert sand particles, where ITZ is weakened by the presence of shrinkage-induced cracking [34]. However, the growth of hydration products at the interface of the ceramic fragments requires suitable composition of ceramic clay, adequate firing temperature, wet environment to promote the reaction and also a significant amount of time [28].

6. Conclusions

The presented paper provides a coupled micromechanical and chemical study on ITZ between fragments of crushed bricks and the surrounding matrix in historic lime-based mortar containing crushed brick particles, known as cocciopesto. The sample from the late Byzantine church built approximately in 9th century in the district Üsküdar, located in Istanbul, Turkey, was used for the analysis.

It has been suggested by many authors that the brick-matrix interface is characterized by the formation of hydration products and it was assumed that this fact can explain the remarkable earthquake resistance and durability of masonry structures having cocciopesto as the bed-joint mortar.

In our work, the formation of hydration products and their stiffness at the interface of the crushed brick fragments was at first analyzed by SEM-BSE, and the micro chemical analysis was accomplished by means of SEM-EDX. The SEM analyzes revealed the reaction rims with reduced porosity at the boundary of crushed brick fragments in the thickness up to 200 μm due to filling of voids by CaO. The presence of hydration products (aluminosilicates) that reinforce ITZ was also detected in a thickness of 20–30 μm around the fragments, documented by the slight increase in aluminum and silicon compounds.

The paper further contains results from mechanical quantification of ITZ investigated by means of grid nanoindentation. It was proven that the interface is reinforced due to increased elastic stiffness compared to the bulk matrix. It was found that there is a steep

stiffness gradient within ITZ, located in a narrow band having the thickness also 20–30 μm. The derived ITZ thickness supports SEM-EDX findings and shows the mechanical enhancement by hydration products in the detected zone. The effect of reduced porosity in this area detected by SEM-BSE further supports the idea of ITZ stiffness enhancement. The average ITZ Young's modulus was approximately 18.4 GPa, which corresponds to the stiffness of low-density CSH found in cement-based composites.

Acknowledgments

The authors wish to thank Prof. Miloš Drdácký for providing the investigated mortar samples, Veronika Petráňová and Antonín Zeman of ITAM for their fruitful collaboration, and Jan Zeman of CTU in Prague for a number of valuable suggestions during the paper preparation. The support of Ministry of Culture of the Czech Republic under the Project NAKI, No. DF11P01OVV008 is also gratefully acknowledged.

References

[1] Arizzi A, Cultrone G. Aerial lime-based mortars blended with a pozzolanic additive and different admixtures: a mineralogical, textural and physical-mechanical study. Construct Build Mater 2012;31:135–43.
[2] Lanas J, Pérez Bernal J, Bello M, Alvarez Galindo J. Mechanical properties of natural hydraulic lime-based mortars. Cement Concr Res 2004;34:2191–201.
[3] Velosa A, Rocha F, Veiga R. Influence of chemical and mineralogical composition of metakaolin on mortar characteristics. Acta Geodynam Geomater 2009;153:121–6.
[4] Cabrera J, Rojas M. Mechanism of hydration of the metakaolin–lime–water system. Cement Concr Res 2000;31:177–82.
[5] Farci A, Floris D, Meloni P. Water permeability vs. porosity in samples of Roman mortars. J Cultural Herit 2005;6:55–9.
[6] Moropoulou A, Bakolas A, Anagnostopoulou S. Composite materials in composite structures. Cement Concr Compos 2005;27:295–300.
[7] Stefanidou M, Pachta V, Konopissi S, Karkadelidou F, Papayianni I. Analysis and characterization of hydraulic mortars from ancient cisterns and baths in Greece. Mater Struct 2013. http://dx.doi.org/10.1617/s11527-013-0080-y.
[8] Sbordoni-Mora L. Les matériaux des enduits traditionnels. In: Proceedings of the ICCROM symposium on mortars, cements and grouts used in the conservation of historic buildings, Rome; 1981. p. 375–83.
[9] Degryse P, Elsen J, Waelkens M. Study of ancient mortars from Sagalassos (Turkey) in view of their conservation. Cement Concr Res 2002;21:1457–63.
[10] Moropoulou A, Cakmak A, Biscontin G, Bakolas A, Zendri E. Advanced Byzantine cement based composites resisting earthquake stresses: the crushed brick/lime mortars of Justinians Hagia Sophia. Construct Build Mater 2002;16:543–52.
[11] Böke H, Akkurt S, Ípekoglu B, Ugurlu E. Characteristics of brick used as aggregate in historic brick-lime mortars and plasters. Cement Concr Res 2006;36:1115–22.
[12] Moropoulou A, Bakolas A, Bisbikou K. Investigation of the technology of historic mortars. J Cultural Herit 2000;1:45–58.
[13] Elsen J. Microscopy of historic mortars: a review. Cement Concr Res 2006;36:1416–24.
[14] Hughes J, Trtik P. Micro-mechanical properties of cement paste measured by depth-sensing nanoindentation: a preliminary correlation of physical properties with phase type. Mater Character 2004;53:223–31.
[15] Constantinides G, Ulm F. The effect of two types of C-S-H on the elasticity of cement-based materials: results from nanoindentation and micromechanical modeling. Cement Concr Res 2004;34:67–80.
[16] Němeček J, Králík V, Vondřejc J. Micromechanical analysis of heterogeneous structural materials. Cement Concr Compos 2013;36:85–92.
[17] Tesárek P, Němeček J. Microstructural and micromechanical study of gypsum. Chemické listy 2011;105:852–3.
[18] Tesárek P, Plachý T, Ryparová P, Němeček J. Micromechanical properties of different materials on gypsum basis. Chemické listy 2012;106:547–8.
[19] Ulm F-J, Vandamme M, Bobko M, Ortega J. Statistical indentation techniques for hydrated nanocomposites: concrete, bone, and shale. J Am Ceram Soc 2007;90:2677–92.
[20] Sorelli L, Constantinides G, Ulm F-J, Toutlemonde F. The nano-mechanical signature of ultra high performance concrete by statistical nanoindentation techniques. Cement Concr Res 2008;38:1447–56.
[21] Neubauer C, Jennings H, Garboczi E. A three-phase model of the elastic and shrinkage properties of mortar. Adv Cement Based Mater 1996;4:6–20.
[22] Nežerka V, Zeman J. A micromechanics-based model for stiffness and strength estimation of cocciopesto mortars. Acta Polytech 2012;52:29–37.
[23] Bakolas A, Aggelakopoulou E, Moropoulou A. Evaluation of pozzolanic activity and physico-mechanical characteristics in ceramic powder-lime pastes. J Therm Anal Calorimetry 2008;92:345–51.
[24] Kramar S, Zalar V, Urosevic M, Körner W, Mauko A, Mirtič B, et al. Mineralogical and microstructural studies of mortars from the bath complex of the Roman villa rustica near Mošnje (Slovenia). Mater Character 2011;62:1042–57.
[25] Silva J, Brito de J, Veiga R. Incorporation of fine ceramics in mortars. Construct Build Mater 2009;23:556–64.
[26] Němeček J. Creep effects in nanoindentation of hydrated phases of cement pastes. Mater Character 2009;60:1028–34.
[27] Lawrence R, Mays T, Rigby S, Walker P, D'Ayala D. Effects of carbonation on the pore structure of non-hydraulic lime mortars. Cement Concr Res 2007;37:1059–69.
[28] Nežerka V, Slížková Z, Tesárek P, Plachý T, Frankeová D, Petráňová V. Comprehensive study on microstructure and mechanical properties of lime-pozzolan pastes. Cement Concr Res 2014;64:17–29.
[29] Vejmelková E, Keppert M, Keršner Z, Rovnaníková P, Černý R, et al. Mechanical, fracture-mechanical, hydric, thermal, and durability properties of lime-metakaolin plasters for renovation of historical buildings. Construct Build Mater 2012;31:22–8.
[30] Oliver W, Pharr G. An improved technique for determining hardness and elastic modulus using load and displacement sensing indentation experiments. J Mater Res 1992;7:1564–83.
[31] Baronio G, Binda L, Lombardini N. The role of brick pebbles and dust in conglomerates based on hydrated lime and crushed bricks. Construct Build Mater 1997;11:33–40.
[32] Herve E, Zaoui A. n-Layered inclusion-based micromechanical modelling. Int J Eng Sci 1993;31:1–10.
[33] Moropoulou A, Cakmak A, Lohvyn N. Earthquake resistant construction techniques and materials on Byzantine monuments in Kiev. Soil Dynam Earthquake Eng 2000;19:603–15.
[34] Nežerka V, Tesárek P, Zeman J. Fracture-micromechanics based model of mortars susceptible to shrinkage. Key Eng Mater 2014;592–593:189–92.